



CHORUS

This is the accepted manuscript made available via CHORUS. The article has been published as:

Thermopower-conductivity relation for distinguishing transport mechanisms: Polaron hopping in CeO_2 and band conduction in SrTiO_3

Stephen Dongmin Kang, Maxwell Dylla, and G. Jeffrey Snyder

Phys. Rev. B **97**, 235201 — Published 6 June 2018

DOI: [10.1103/PhysRevB.97.235201](https://doi.org/10.1103/PhysRevB.97.235201)

Thermopower-conductivity relation for distinguishing transport mechanisms: polaron hopping in CeO_2 and band conduction in SrTiO_3

Stephen Dongmin Kang,^{1,2,*} Maxwell Dylla,² and G. Jeffrey Snyder^{2,†}

¹*Department of Applied Physics and Materials Science,
California Institute of Technology, CA 91125, USA*

²*Department of Materials Science and Engineering, Northwestern University, IL 60208, USA*

The charge transport mechanism in a solid is often inferred by observing very simple features like the temperature dependency of electrical conductivity or resistivity. However, comparing complicated physical models to such simple signatures leaves much ambiguity. Because models generally have more parameters than the types of measurements available, inconsistencies can long go unrecognized until the interrelation between different measurements is closely examined. We show that a simple investigation of the thermopower-conductivity relation allows one to phenomenologically characterize transport from experiments; the phenomenologically determined transport function can be compared to physical models to distinguish transport mechanisms and straightforwardly point out inconsistencies in literature models. We highlight two example cases, ceria and strontium titanate, to show that our analysis method can clarify whether the transport mechanism is through hopping or delocalized states. We question previous suggestions about the scattering mechanism in SrTiO_3 and suggest deformation potential scattering on elongated Fermi surfaces as the origin of high temperature T^2 resistivity.

I. INTRODUCTION

Physically interpreting low and thermally activated electronic conductivity in crystalline semiconductors (which is often the case for metal oxides) is challenging. Viewing charge transport as a hopping process through localized states [1; 2] or propagating Bloch waves [3] has been contentious since the earliest studies [4]. Even in popular materials, such as perovskite oxides, it is still not unusual to find a lack of wide consensus on the charge transport mechanisms. For example, in SrCoO_3 -based derivatives, features of both band conduction [5; 6] and small polaron conduction [7] are found in the direct-current (DC) conductivity, inviting further investigation. A reliable analysis method for determining the relevant conduction mechanism is not straightforwardly established in the literature. Typically, analysis is centered on the temperature dependence of conductivity; however, it is challenging to deconvolute and distinguish various physical processes that are thermally activated by only studying conductivity. Here, we propose that the thermopower-conductivity relation could be used as a simple but powerful means to study transport mechanisms. Thermopower and conductivity are properties that are determined by an identical underlying transport function, each sampled with different spectral weighting. Using the transport function determined by the interrelation of two different measured properties is extremely useful for testing models. We demonstrate how this method can be applied to identify n-type SrTiO_3 as a band conductor and oxygen deficient CeO_2 as a small polaron conductor.

II. AMBIGUITY IN INTERPRETING THE TEMPERATURE DEPENDENCY OF CONDUCTIVITY

The biggest reason why the temperature dependence of DC conductivity $\sigma(T)$, by itself, does not provide an unambiguous mechanistic signature is because different physical processes exhibit similar features. The most common example of this ambiguity is thermal activation; although small polaron hopping and band conduction are completely different physical descriptions, they give rise to similar thermal activation behavior. As a simple example, contrast transport from a non-degenerate band conductor, where the Fermi-level E_F is more than a few $k_B T$ away from the band edge (Fig.1a), and a polaron hopping conductor (Fig.1b). In a non-degenerate band conductor, exponential thermal activation $\exp\left(\frac{E_F - E_t}{k_B T}\right)$ is observed due to the temperature dependence of the

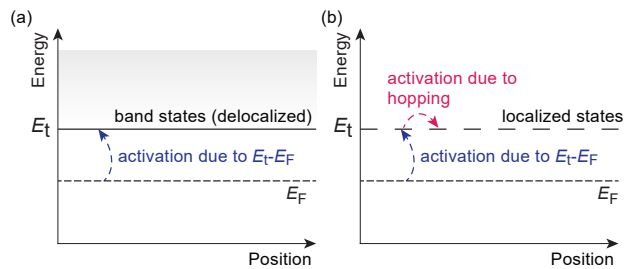


FIG. 1. Contributions to thermally activated conduction. **(a)** Band conductor. Thermally activated behavior results from the Fermi-level being away from the band states. **(b)** Hopping conductor. The transport process between localized states, by itself, is also a thermally activated process. It is often not straightforward to distinguish the two origins by simply analyzing the temperature dependence of conductivity.

carrier concentration (in the terminology of the Drude model). In this case, the band edge plays the role of a phenomenological “transport edge E_t .” In a polaron hopping conductor, transport occurs through localized states, which are different than band states, but serve as a phenomenologically identical transport edge E_t . Thus, $\exp\left(\frac{E_F - E_t}{k_B T}\right)$ behavior is observed in this case as well, despite the transport mechanism being different. Additionally, transport between localized states is also thermally activated, which is typically referred to as “activated mobility” such as $\mu \propto \frac{1}{T} \exp\left(-\frac{E_a}{k_B T}\right)$, where E_a is an activation energy. Hopping conductivity would be observed with a combined contribution from the two processes.

In the general case for hopping, the carrier activation and mobility activation could be more convoluted than the simple example above. Carrier activation in heavily doped materials requires use of the Fermi-Dirac distribution rather than an exponential function. Mobility does not necessarily follow an exponential dependency either [1; 8]; in both percolation models and variable range hopping models [1], the temperature dependency is $C(T) \cdot \exp\left[\left(-\frac{E_{av,\gamma}}{k_B T}\right)^\gamma\right]$, where γ is an exponent that is generally associated with dimensionality. The prefactor $C(T)$ also depends on temperature, although weakly in comparison to the exponential term.

An additional source of thermal activation in transport is the grain boundary effect [9]. Although avoiding such complications from the perspective of understanding the intrinsic charge transport mechanism is desirable, grain boundary effects more than often dominate the behavior of $\sigma(T)$. Dominance of the grain boundaries is, in a sense, inevitable in polycrystalline materials, especially in dielectrics where space charges cannot be screened very well by charges [10]. Single crystals, if available, are advantageous in ruling out such extrinsic effects.

Optical measurements sometimes help disentangle the various causes of thermal activation behavior, but analyzing these measurements present additional challenges. For example, signatures in optical measurements could be associated with the presence of polarons [2; 11–13], although with challenges in the interpretation. However, the mere presence of polarons, or their contribution to optical conductivity, does not warrant that they significantly contribute to the DC charge transport behavior.

Ambiguity in $\sigma(T)$ is an issue not only for thermal activation. For example, when determining scattering mechanisms in band conductors, $\sigma(T)$ can be different than model predictions due to a temperature-dependent E_F (which can be significant even for a fixed carrier concentration because of thermal broadening, especially at intermediate doping levels). Even for a well-resolved temperature dependency such as $\sigma \propto T^n$, n could correspond to multiple physical mechanisms that are indistinguishable with σ itself. Similar issues are encountered in the analysis of any type of mobility.

III. ANALYSIS METHOD USING THE THERMOPOWER-CONDUCTIVITY RELATION

The basic idea underlying thermopower-conductivity analysis is to determine a general and phenomenological transport function that does not depend on a particular physical model. The thermopower-conductivity relation found from experiments allows one to identify the phenomenological transport function, which can then be compared to mechanistic transport functions derived from physical models.

The transport function $\sigma_E(E)$ is an energy-dependent function that yields conductivity when integrated over energy while taking into account the Fermi-Dirac distribution f :

$$\sigma = \int \sigma_E(E) \left(-\frac{df}{dE}\right) dE. \quad (1)$$

Here, $-df/dE$ is a peak function centered at E_F , taking care of the fact that fermions need empty states in order to be transported. In terms of a physical interpretation, $\sigma_E(E)$ can be understood as the capability to conduct at each energy level. Use of f indicates that, when electron interactions are non-negligible, $\sigma_E(E)$ is an effective quasiparticle description (analogous to, for example, renormalized band structures of heavy fermion systems). When $\sigma_E(E)$ represents only one type of carrier, the Seebeck coefficient is:

$$S = \left(\frac{k_B}{q}\right) \frac{1}{\sigma} \int \sigma_E(E) \left(\frac{E - E_F}{k_B T}\right) \left(-\frac{df}{dE}\right) dE, \quad (2)$$

where, q is the charge of the carrier ($-e$ for electrons). It is seen that $\sigma_E(E)$ determines both σ and S for a given E_F . Therefore, by finding the $S - \sigma$ relation by changing E_F , one can deduce the functional form of $\sigma_E(E)$ that governs charge transport.

The $S - \sigma$ relation can be largely divided into two cases: when charge is transported through a very narrow energy channel or through a dispersive spectrum. We show that these cases are easily distinguishable by studying the $\log |S| - \log \sigma$ plot.

A. Narrow Transport Function

When the energy distribution of states participating in transport is narrow relative to $k_B T$, the transport function can be approximated as a Dirac delta function:

$$\sigma_E(E) = A_t \cdot \delta(E - E_t), \quad (3)$$

where A_t is an energy-independent coefficient. Narrow transport is typically associated with transport through localized states (no dispersion) such as small polarons [14]. Hopping transport models [1; 15; 16] that use the so-called transport energy (an energy level statistically representing the overall transport [17]) are mathematically

equivalent to using a narrow transport function. Even in variable range hopping models that envision hopping through states of varied energy levels, calculating transport for a single transport energy level makes the model equivalent to using a narrow transport function.

By using Eqs. 1 and 2, and by setting $c = f(E_t - E_F)$ and $\sigma_{E_0} = A_t/k_B T$,

$$\sigma = \sigma_{E_0} \cdot c(1 - c), \quad (4)$$

and

$$S = \frac{E_t - E_F}{qT} = \frac{k_B}{q} \cdot \ln\left(\frac{1 - c}{c}\right). \quad (5)$$

Here, σ_{E_0} , is a transport coefficient in the units of conductivity that determines the magnitude of conductivity for a given E_F , and c is the occupancy of the transport states. Eqs. 4 and 5 are referred to as the Heikes equations in the literature, but here it is derived without assuming the absence of spin nor an infinite temperature (to neglect kinetic terms) [18; 19]. Mathematically, the infinite temperature assumption used in [18; 19] is equivalent to a narrow transport function assumption; for interpreting experimental data at a given temperature, it is more relevant to understand the assumption in terms of the width of the transport function relative to $k_B T$.

If one defines c' as site occupancy (instead of transport state occupancy) and considers that each site can accommodate both spin up and down, then $c' = 2f = 2c$. Conductivity and the Seebeck coefficient become:

$$\sigma = \sigma_{E_0} \cdot \frac{c'}{2} \left(1 - \frac{c'}{2}\right), \quad (6)$$

and

$$S = \frac{k_B}{q} \cdot \ln\left(\frac{2 - c'}{c'}\right). \quad (7)$$

In the literature, Eq. 7 has been suggested as a necessary modification in the Heikes equation to take into account spins [4; 18; 19]. This distinction could be important when estimating c or c' based on other quantities like vacancy concentration; however, the distinction does not affect the $S - \sigma$ relation.

The $S - \sigma$ relation for narrow transport is found by eliminating c in Eqs. 4 and 5:

$$\frac{\sigma}{\sigma_{E_0}} \left[1 + \exp\left(\frac{S}{k_B/q}\right)\right] \left[1 + \exp\left(\frac{-S}{k_B/q}\right)\right] = 1. \quad (8)$$

This relation is identically found from Eqs. 6 and 5. It is seen that the $S - \sigma$ relation is fixed for narrow transport except for a scaling factor σ_{E_0} .

Temperature dependence of the Seebeck coefficient can be used to support the conclusion of a narrow transport function. When the number of charge carriers is extrinsically fixed in a material (*e.g.* a fixed defect concentration while having no bipolar excitations), thermopower becomes temperature independent for a narrow density of

states, as suggested by Eq. 5. This independence results from the Fermi-level self-adjusting with temperature in a way that gives a constant reduced Fermi-level. Suppose that the number of electrons provided by defects or dopants is fixed at n_0 . Then, the Fermi-level would be determined by:

$$n_0 = \int g(E) f\left(\frac{E - E_F}{k_B T}\right) dE, \quad (9)$$

where $g(E)$ is the density of states. When the density of states is a narrow function around E_t , $g(E) \approx N \cdot \delta(E_t)$. As a result:

$$n_0 \approx N \cdot f\left(\frac{E_t - E_F}{k_B T}\right) = N \cdot f(-\eta). \quad (10)$$

Therefore, when $c = n_0/N$ is fixed with respect to temperature, η is also fixed (*i.e.* E_F shifts in a way that keeps η constant), making S temperature-independent. Note that when the narrow band states are the dominant conductive states but are not the only states controlling η (*e.g.* non-conductive states below the narrow band), a weakly temperature-dependent S could be observed despite transport being governed by a narrow band.

B. Dispersive Transport Function

When the states that participate in transport are dispersive in energy, the transport function is often well-described with a power law above a transport edge:

$$\begin{aligned} \sigma_E(E) &= \sigma_{E_0} \cdot \left(\frac{E - E_t}{k_B T}\right)^s & (E \geq E_t) \\ &= 0. & (E < E_t) \end{aligned} \quad (11)$$

The exponent s depends on the particular transport mechanism and σ_{E_0} is again used as a transport coefficient in the units of conductivity. Dispersive transport is typically associated with transport through delocalized band states (with possible exceptions [20]). Most archetype band transport models for σ and S are equivalent to Eq. 11 with σ_{E_0} and s corresponding to particular physical parameters of the model and the overall energy exponent, respectively.

By using Eqs. 1 and 2:

$$\sigma = \sigma_{E_0} \cdot s F_{s-1}(\eta), \quad (12)$$

and

$$S = \left(\frac{k_B}{q}\right) \left[\frac{(s+1)F_s(\eta)}{sF_{s-1}(\eta)} - \eta\right]. \quad (13)$$

Here, $\eta = (E_F - E_t)/k_B T$ is the reduced Fermi-level and $F_i(\eta) = \int_0^\infty \frac{t^i}{\exp(t-\eta)+1} dt$ is the complete Fermi integral.

Extracting the $S - \sigma$ relation requires numerical integration of Eqs. 12 and 13, parameterized by η . The

relation is fixed for a given s except for a scaling factor σ_{E_0} , allowing one to deduce s from the relation. In the limit where $\eta \gg 1$, the $S - \sigma$ relation can be obtained analytically using the Sommerfeld expansion:

$$S = \frac{k_B \pi^2}{q} s \left(\frac{\sigma}{\sigma_{E_0}} \right)^{-1/s}. \quad (14)$$

It is seen that a $\log |S| - \log \sigma$ plot is most useful in distinguishing s because the linear slope converges to $-1/s$ as η increases. In the opposite limit ($\eta \ll -1$), all mechanisms (even the narrow transport case) become an identical form of $S \propto \log \sigma + \text{constant}$, making them indistinguishable by only using the $S - \sigma$ relation [20].

Next, we note how different scattering models for band transport can be mapped to the phenomenological exponent s . For semiclassical band conduction [3], $\sigma_E(E)$ from a particular band is:

$$\sigma_E(E) = q^2 \cdot v^2(E) \tau(E) g(E), \quad (15)$$

where v is the velocity and τ is the relaxation time of charge carriers. For deformation potential scattering models including acoustic phonon scattering [21], non-polar optical phonon scattering [22], and intervalley scattering [23], $\tau(E) \propto g^{-1}(E)$; thus, $v^2(E)$ determines s in this case, giving $s = 1$ for free electron-like behavior.

Through similar arguments, polar-optical phonon scattering corresponds to $s = 2$ [22] and ionized impurity scattering corresponds to $s = 3$ [24]. Point defect scattering is another case that gives $s = 1$ [25]. These differences result from additional energy dependencies in τ calculated from each scattering model, from which the leading order energy term is taken.

When band complexity is involved, such as secondary bands contributing to transport [26], the $\sigma_E(E)$ also becomes more complex than a simple power law. Such complexity is analogous to effective mass becoming a more complex function than a constant. See Ref.[27] for a more detailed discussion.

IV. APPLICATION TO MATERIALS

A. Polaron hopping in CeO_{2-x}

Ceria is a material widely used for its promising oxygen redox properties [29; 30]. The strong electronic contribution to conductivity in ceria makes it especially advantageous for electrocatalysis [31]. The mechanism by which charge is transported has been described as small polaron conduction [28; 32], but the analysis depended on assumptions about polaron state occupancy [28; 32] or debatable data corrections [32]. In this section, it is shown that the identical conclusion can be reached through a more straightforward route of analyzing the $S - \sigma$ relation at a given temperature.

The $\log |S| - \log \sigma$ relation observed in single crystal CeO_{2-x} at 1273 K follows that predicted by a narrow

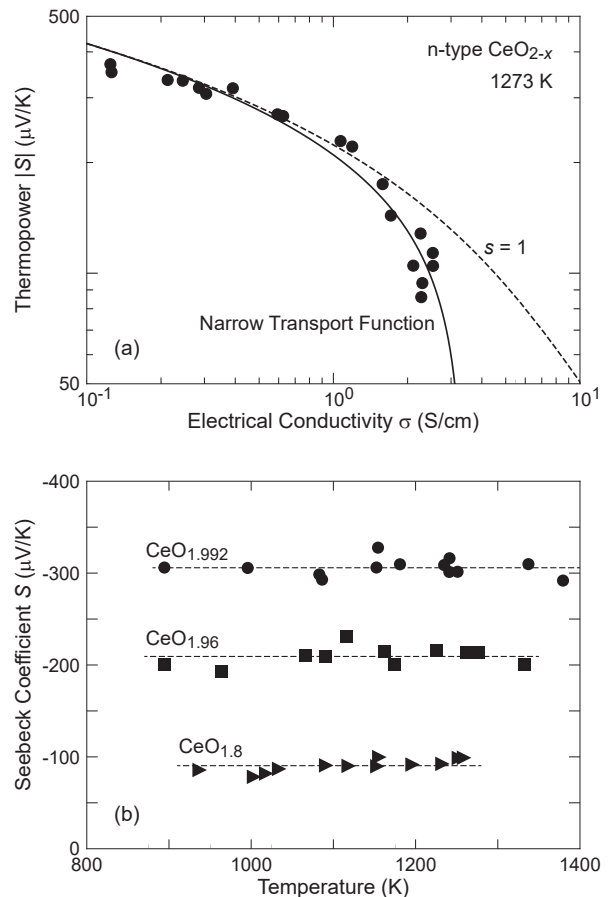


FIG. 2. (a) Analysis of the $\log |S| - \log \sigma$ relation at 1273 K in single crystal n-type CeO_{2-x} reduced to different compositions by atmosphere control, using data from Ref.[28]. The data indicate that a narrow transport function is governing the transport in this material. To find the Seebeck coefficient corresponding to each conductivity measurement, the Seebeck coefficient versus composition data were fitted to find an empirical relation. (b) Temperature dependency of the Seebeck coefficient as compiled in the same reference. The dashed lines are guides to the eye showing the average value with respect to temperature.

transport function (Eq. 3), which is significantly different than what is predicted by band transport (Fig. 2a). A narrow transport function is consistent with hopping conduction through small polarons. Since this analysis is done at a fixed temperature, concerns with the complicated phase diagram of CeO_{2-x} is avoided by simply picking a temperature at which CeO_{2-x} is a single phase (fluorite) over a wide off-stoichiometry range.

We note that estimations of polaron occupancy (c for Eqs. 4-5 or c' for Eqs. 6-7), or even composition, is not explicitly required for the analysis in Fig. 2a. It is more reliable to not explicitly use c (or c'), as in analyzing $S(c)$ or $\sigma(c)$, because of the ambiguity or uncertainty of how c corresponds to a particular composition. As long as it is experimentally established how a particular S corre-

sponds to a particular σ , the transport function can be inferred from $S - \sigma$ without further assumptions about, for example, polaron states. This advantage of analyzing $S - \sigma$ is analogous to not requiring information about the carrier concentration when studying band conductors.

From the temperature dependency of thermopower, it can be inferred that the narrow transport function description persists at temperatures other than 1273 K (at which $\log |S| - \log \sigma$ was analyzed). In Fig. 2b, it is seen that the thermopower of CeO_{2-x} (fixed x) is insensitive to temperature. In this measurement, the composition of CeO_{2-x} was fixed by equilibrating with a predetermined reducing atmosphere and then quenching to lower temperatures. Since the electrons are provided by the oxygen vacancies in CeO_{2-x} , fixing the composition is equivalent to fixing c . Therefore $S(T)$ is consistent with the $\log |S| - \log \sigma$ relation found at 1273 K. In such situations where the $\log |S| - \log \sigma$ relation cannot be fully examined at some temperatures (in ceria it is due to the limited range of off-stoichiometry at lower temperatures), temperature dependency is a useful way to see whether the transport function description found at one temperature could be a reasonable description at other temperatures.

B. Band conduction in SrTiO_3

Strontium titanate (SrTiO_3) is one of the most widely studied perovskites for its electronic properties [35–37]. SrTiO_3 has been widely recognized as a band conductor in the literature [33; 34; 38–42], with only a number of reports citing hopping conduction from the activated conductivity in polycrystals [43–46]. Nevertheless, precisely how band conduction should be justified and what models should be used to quantitatively analyze transport measurements are topics with not much consensus; found in the literature are mixed assessments on the scattering mechanisms including ionized impurity scattering [33; 38], deformation potential scattering [34], and polar optical phonon scattering [34]. Here, we show through a Seebeck-conductivity analysis that doped n-type SrTiO_3 , at 120 K and above, phenomenologically follows the $s = 1$ dispersive transport model curve, which is consistent with band conduction through deformation potential scattering.

The experimental $\log |S| - \log \sigma$ relation in n-type doped SrTiO_3 agrees very well with the $s = 1$ curve (Fig. 3). By contrast, the curve predicted for a narrow transport function shows a steeper decrease in thermopower when $|S| < 300 \mu\text{V/K}$. This analysis allows us to unambiguously conclude that the energy dependency of the transport function is $\sigma_E \propto E$ above the transport edge, rejecting the claim of polaron mediated transport in this material.

Identification of the $s = 1$ relation allows us to also exclude polar-optical phonons or ionized impurities as the dominant scattering mechanism for band conduction at > 120 K. Ionized impurity scattering has previously been

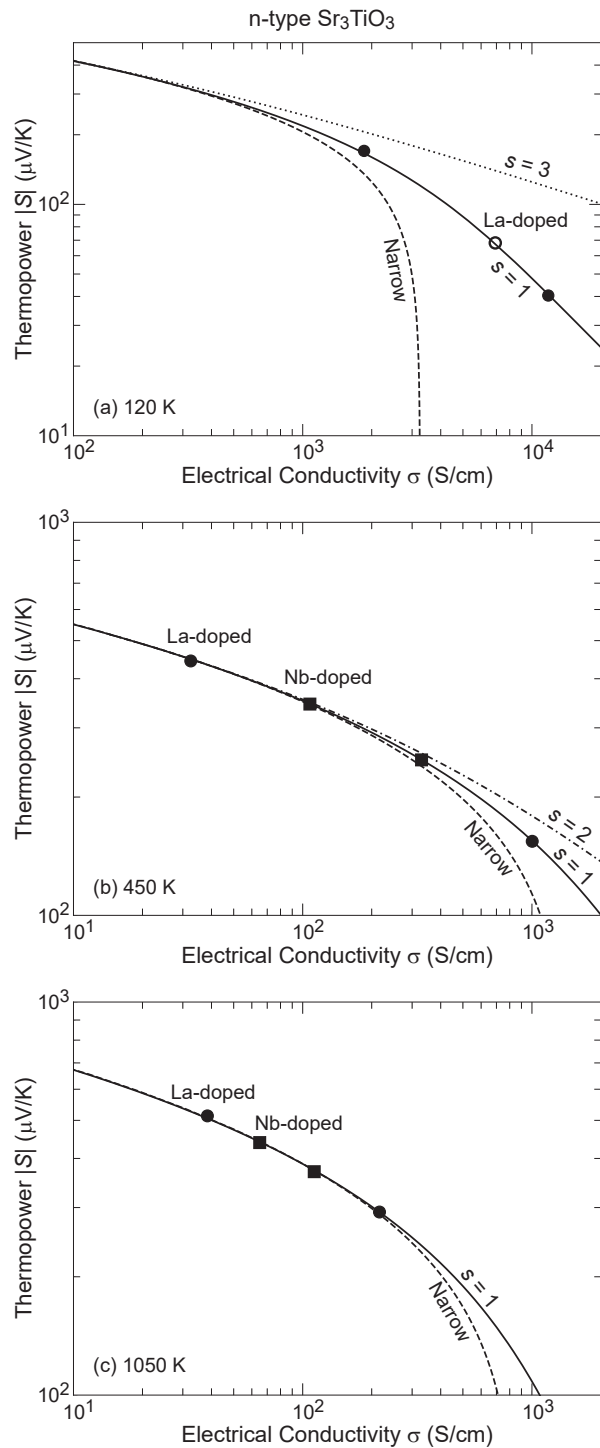


FIG. 3. Analysis of the $\log |S| - \log \sigma$ relation in single crystal n-type SrTiO_3 doped with either La (circles) or Nb (squares): (a) 120 K; (b) 450 K; (c) 1050 K. Best fit is found with $s = 1$ at 120 and 450 K, compared with other exponents corresponding to previous suggestions found in the literature. At 1050 K, the large thermopower of the given data makes it difficult to distinguish between different cases. Data are from Ref.[33] and [34] for (a) and (b-c), respectively. The open marker indicates that conductivity was interpolated from adjacent compositions.

suggested as the low temperature scattering mechanism [33; 38], which, however, would have to appear with a $s = 3$ relation that is not in agreement with measurements at 120 K (Fig. 3a). Polar-optical phonon scattering, which would be $s = 2$, has been suggested for above room temperature [34]; however, at 450 K (Fig. 3b) the $s = 2$ relation does not explain the measurements.

The reason why examining the S - σ relation allows one to easily exclude other mechanisms that have been suggested through different analysis routes is because it is less dependent on assumptions, only requiring a simple scaling behavior of the transport function with respect to energy. For example, in the analysis that has led to suggesting polar-optical phonon scattering using the S - n relation [34] (n is carrier concentration), the Fermi-level was inferred from estimations of n in a way that assumes a particular Fermi surface (one that is reducible to an energy-independent effective mass for the density of states). However, the peculiar shape of the conduction band Fermi surface of SrTiO₃ upsets that approach. For charge transport, on the other hand, only the carriers with a light inertial mass contribute meaningfully; even for a complicated Fermi surface, the carriers dominating transport are often simply described as $v^2 \propto E$, as is the case for SrTiO₃.

Another reason is because one naturally arrives at a phenomenological description that is consistent for both S and σ by examining the S - σ relation. Without directly studying the S - σ relation, the inconsistency between S and σ in a model is easily missed, as exemplified in the SrTiO₃ literature.

Two questions still remain from the analysis in Fig. 3. First, whether it is reasonable to consider 1050 K to be $s = 1$, where model lines are indistinguishable due to the increased thermopower at high temperature (Fig. 3c). Second, whether the deformation potential scattering model, which is what $s = 1$ would typically indicate, is consistent with the temperature dependency of transport observed in SrTiO₃. These questions can be addressed by extracting the temperature dependent relaxation time of charge carriers.

Converting σ_{E_0} , the phenomenological transport coefficient which determined only the magnitude of conductivity in Fig. 3, into a carrier relaxation time τ requires a physical model. Here, we use a semiclassical band conduction model that takes into account the 2D-like Fermi surface features of n-type SrTiO₃. From the model derived in the Appendix, the mechanistic transport function for SrTiO₃ can be specified in terms of band conduction parameters:

$$\sigma_E(E) = \frac{2e^2 k_B T}{a\pi\hbar^2} \tau(T) \cdot \frac{E - E_t}{k_B T}, \quad (E \geq E_t) \quad (16)$$

where $-e$ is the charge of an electron, a is the lattice constant, and $\tau(T)$ is the relaxation time of the light carriers, which dominate transport, and dependent on temperature but not energy. The extracted relaxation time plotted in Fig. 4 shows that samples with different levels

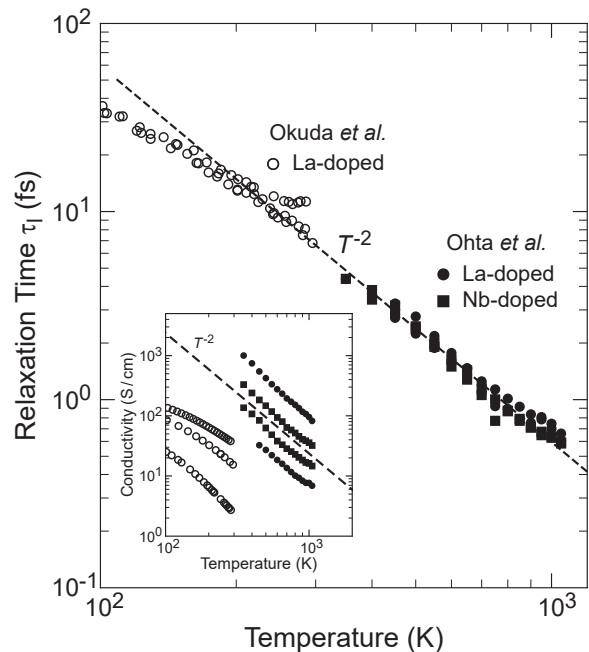


FIG. 4. The temperature dependent relaxation time of the carriers dominating transport in n-type single crystal SrTiO₃, extracted from thermopower and conductivity using the model Eq. 16. A dashed line representing T^{-2} is drawn for comparison. The inset shows the original conductivity data used for extracting the relaxation times. The collapse of different conductivity curves onto a single relaxation time curve indicates the energy independence of τ_1 , which is consistent with the 2D character of transport. High and low temperature data are from Ref.[34] and Ref.[33], respectively. The lattice constant was fixed at $a = 3.905 \text{ \AA}$ [48] for the calculation.

of doping collapse onto a single curve, indicating that the energy independent relaxation time characteristic of a 2D density of states is indeed a reasonable description for the dominant charge carriers in SrTiO₃. This description is also consistent with experiments where τ was observed to be independent of carrier concentration [47].

The relaxation time in Fig. 4 does not show notable signs of a crossover in the temperature dependency above 450 K. This monotonic behavior indicates that the $s = 1$ relation found at 120-450 K is most likely applicable also at higher temperatures; for a change in s , the temperature dependency would also change. We note that although the quantification of τ relies on the physical model (Eq. 16), the absence of a crossover is a phenomenological feature (*i.e.* model-independent).

Next, we explain why the physical origin of $s = 1$ could be attributed to deformation potential scattering in n-type SrTiO₃. In Fig. 4, τ converges to T^{-2} at high temperature. This dependency might seem different than the typical $\tau \propto T^{-1}$ expected for deformation potential scattering at high temperatures [21; 49]. However, as has been studied for the case of Bi, a cylinder-like Fermi surface (elongated Fermi surface) results in $\tau \propto T^{-2}$ in a temperature range where the phonon wave vectors exceed

the diameter of the cylindrical Fermi surface ($T > T_D$) while still being smaller than the length of the cylinder ($T < T_L$) [49; 50]. n-type SrTiO₃ fits well into this criteria. The SrTiO₃ Fermi-surface can be decomposed into three elongated ellipsoids, and we can consider the T^{-2} regime of each ellipsoid. The lower temperature bound increases with E_F ; for the highest doping sample ($S \approx 40 \mu\text{V/K}$ sample at 120 K in Fig. 3), $T_D \approx 180$ K for acoustic phonons (speed of sound of $v_s = 7900$ m/s and $m_1^* = 1.1m_e$ assumed for this estimation). The cylinder length (or long axis of the ellipsoid) of the Fermi-surface in n-type SrTiO₃ is similar to the Brillouin zone itself, so the upper temperature T_L for acoustic phonons is limited by the Debye temperature along that direction (485 K using $v_s = 7900$ m/s). On the other hand, the dispersive optical phonon branches in SrTiO₃ [51] will play a similar role (optical deformation potential due to long range optical phonons), but with a much higher T_L and lower T_D . Thus, continuation of T^{-2} at $T > 485$ K could indicate contribution from optical deformation potentials. Overall, deformation potential scattering offers a good explanation for the $\tau \propto T^{-2}$ found in the heavily doped n-type SrTiO₃ samples (Fig. 4). Both the temperature dependency ($\tau \propto T^{-2}$) and energy dependency ($s = 1$) of the transport function being consistent with deformation potential scattering strongly suggests that the physical description is proper.

We note that many transition metal perovskite oxides have Fermi surfaces similarly elongated along three axes; indeed, many literature examples such as PrNiO₃ [52], KTaO₃ [53], SrNbO₃ [54], and SrMoO₃ [55] are found with a resistivity $\propto T^2$ at temperatures not very low. The relation between deformation potential scattering on elongated Fermi surfaces and the T^2 resistivity has not yet been considered previously in those materials.

A mechanism that is commonly associated with the $\tau \propto T^{-2}$ is electron-electron scattering emerging from Fermi-liquid behavior, which has been discussed for SrTiO₃ at low temperatures < 100 K [56]. It is unclear whether electron-electron scattering is consistent with $s = 1$. Above all, it is questionable whether electron-electron scattering should dominate over deformation potential scattering at temperatures as high as 1000 K. Difficulties in Fermi-liquid theory for explaining the high temperature conduction in a number of metal oxide perovskites have also been discussed in [47].

Overall, the observed $s = 1$ relation in single crystals concludes the transport mechanism in n-type SrTiO₃ to be band conduction as opposed to polaron hopping. The band conduction mechanism is found to be consistent with deformation potential scattering if one takes into account the shape of the Fermi surface elongated along each axis. The thermally activated conduction behavior observed in some polycrystalline samples [43–46] should be attributed to grain boundary effects rather than an intrinsic conduction mechanism of SrTiO₃. Finally, it should be noted that in pure and stoichiometric SrTiO₃, where the extrinsic or self-doping level is extremely low,

the conductivity due to band conduction could be low enough to make polaron hopping conduction possibly the dominant transport mechanism [57; 58].

V. COMPARISON WITH OTHER ANALYSIS METHODS

A. Use of the Temperature Dependency of the Seebeck coefficient

The temperature dependency of S , on its own, only provides limited information about the transport mechanism because it is more related to the statistical shift of the Fermi-level. For example, in conductors with a dispersive transport function in the degenerate limit, $S = \frac{k_B}{q} \frac{\pi^2}{3} \frac{s}{\eta} \propto T$ regardless of the exponent s .

The temperature-independent S of the narrow transport case does provide a clearer indication. However, any additional states that do not participate in transport but still affect the statistical shift of the Fermi-level will give rise to weak temperature dependency.

B. Use of Hall Measurements

Hall measurements, in contrary to the common belief, mostly do not provide additional information in determining the transport function. This argument can be understood by considering band conductors as an example. The Hall coefficient from a particular band can be expressed in terms of the transport function:

$$R_H = \frac{1}{\sigma^2} \int \left(\frac{q\tau}{m^*} \right) \sigma_E(E) \left(-\frac{df}{dE} \right) dE. \quad (17)$$

Here, m^* is the effective mass of the particular band under consideration. It is seen that R_H requires knowledge of the term $q\tau/m^*$ (which is an energy-dependent function), in addition to $\sigma_E(E)$. For the determination of $\sigma_E(E)$, Hall measurements simply add one measurable and one unknown at the same time. In situations where $\sigma_E(E)$ is already known (transport mechanism already understood), R_H provides information about the electronic structure, which illustrates the rather different purpose served by Hall measurements.

C. Jonker Analysis

Studying the $S - \sigma$ relation on a S vs. $\log \sigma$ plot (Jonker plots) is a useful way of extracting information about the band gap and weighted mobilities [59]. However, the linear S (rather than $\log S$) scale is more relevant for investigation of the non-degenerate limit, in which different transport mechanisms cannot be distinguished by only the $S - \sigma$ relation. The idea to use

the Jonker plot for distinguishing band and small polaron transport has been suggested previously [32], but the model description for the degenerate limit was not accurate.

VI. REMARKS ON ASSUMPTIONS

A. On the use of a homogeneous transport function

Decomposing conductivity in energy space using a single transport function such as Eq. 1 is equivalent to treating the material as a homogeneous system. Although this approach can still be used for some chemically inhomogeneous materials when the transport function is effectively homogeneous, inhomogeneity can always be a potential complication in general.

Transport in polycrystalline materials, in contrast to single crystals, is the most common example where inhomogeneity due to the grain boundaries is a potential concern. Grain boundaries inevitably have a different electronic structure than the grain, inducing charge transfer that results in space charge regions that are spatially extended on a scale much larger than that of the grain boundary itself [10]. In some metals, the grain boundary effect is either small (non-significant charge transfer) or screened well enough to be treated as a homogeneously distributed scattering source (which is one assumption behind using Matthiessen’s rule on scattering times like $\tau^{-1} = \sum \tau_i^{-1}$ [60; 61]). This approach is equivalent to using a homogeneous transport function. On the other hand, in some semiconductors or insulators, the grain boundary influence could be significant enough to make it prohibitive for a homogeneous transport function to accurately describe transport, as has been shown in Mg_3Sb_2 [9; 62]. In oxides, grain boundaries generally tend to have a big impact on transport, but the effect can also be mitigated through synthesis routes that produce grain boundaries with a more conductive composition via atmosphere control [63–65]. When mitigated well enough, polycrystalline samples can show $S - \sigma$ relations resembling that of a single crystal [64]. When grain boundaries dominate the resistance of the material and chemical doping changes mostly the grain boundary resistance rather than the Fermi-level, the resulting $\log |S| - \log \sigma$ curve would tend to be flattened out (which should not be attributed to a high s exponent). This tendency is because reduction of the grain boundary does not result in significant changes to the thermopower [9].

As an exceptional case, conducting polymers, which have a highly inhomogeneous microstructure, apparently exhibit transport like a homogeneous transport function [20]. Because such a large variety of polymers with a wide range of doping levels appear to follow an identical transport function, it has speculated that the functional form of the transport function might originate from the microstructural characteristics of the inhomogeneity itself, such as percolation. It is also possible that the ordered

regions of the material simply dominate the energy dependency of the transport function.

Overall, even for inhomogeneous systems, the $\log |S| - \log \sigma$ plot is still a useful means to understand the transport in a material. However, whether the observed behavior represents the inherent single crystal material property is often not necessarily clear for polycrystalline or inhomogeneously ordered materials.

B. On the rigid transport function assumption

Inferring the form of the transport function from a $\log |S| - \log \sigma$ plot requires multiple samples with different Fermi-levels. In oxides, E_F can be controlled either by extrinsic doping or by oxygen off-stoichiometry control. Whether such processes will keep the transport function unchanged could be a challenging question to answer. Largely two different cases should be considered when rethinking the starting assumption of a “rigid” transport function (the term “rigid” originates from the “rigid band assumption” in electronic structure studies).

The first concern is whether the functional form of the transport function is changing as the sample is tuned in order to change E_F . Since a change in the functional form is indicative of a change or crossover in the dominant transport mechanism, accompanying changes that signify the crossover would be observed. For example, crossovers in the temperature dependency of mobility, relaxation time, or σ_{E_0} would indicate possible crossovers in the transport mechanism.

Another concern is the transport coefficient σ_{E_0} being systematically correlated to changes in the E_F , like alloying effects exploited in band engineering [26; 66; 67]. A common example would be a dopant—primarily intended to change the E_F , but not the band itself—also acting as an alloying element to change the band effective mass, such as the case of Fe-substituted SrTiO_3 [39]. This type of breakdown of the rigid transport function is harder to notice because of its continuous and systematic dependence of σ_{E_0} on the chemical substitution; a system with a transport function of $s = 1$ could appear to have a significantly different curve shape in the $\log |S| - \log \sigma$ plot due to a continuously changing σ_{E_0} . For band conductors, measurement of the Hall mobility could help notice such changes, but only if Hall mobility can be straightforwardly converted to an η -independent transport parameter (*e.g.* σ_{E_0} or a mobility parameter such as μ_0 [27]); Hall mobility itself is intrinsically η -dependent in the heavily doped regime even for a rigid transport function. Comparing the effect of multiple types of dopants (*e.g.* comparing Nb and La dopants in SrTiO_3) is a useful way to confirm the validity of a rigid transport function assumption. Investigating the non-degenerate limit, in which the Hall mobility is expected to be constant with respect to E_F for a rigid transport function, is another way to check the rigidity assumption.

Additionally, electron interactions could be a cause for

non-rigid behavior in the transport function [68], making σ_{E_0} dependent on E_F (recall that the transport function was formulated in Eq. 1 using f).

VII. CONCLUSIONS

We have shown that investigation of the $S - \sigma$ relation provides a simple yet powerful means to study the stationary charge transport mechanism in materials. This analysis complements the conventional means of simply testing models with the temperature dependency of $\sigma(T)$ or $S(T)$. Since a given physical transport model almost always predicts both a conductivity and a Seebeck coefficient, testing the $S - \sigma$ relation with experiments naturally tests for a self-consistent model description.

The experimental $S - \sigma$ relation provides a phenomenological transport function $\sigma_E(E)$ that can be easily compared to the mechanistic transport function of physical models. While energy-dependent parameters in a physical model are not easily tested by individually investigating σ or S , $\sigma_E(E)$ directly tests the energy-dependency.

Therefore, the $S - \sigma$ relation should always be studied in addition to conventional means when determining the charge transport mechanism.

Appendix: Transport function for n-type SrTiO₃

A simplified Fermi surface model for the conduction band is useful for studying the transport with an analytical equation. The complex Fermi-surface of n-type SrTiO₃ originates from three interpenetrating prolate ellipsoids along three orthogonal axes that are symmetrically identical. The dispersion relation of one prolate ellipsoid aligned along the z -axis is:

$$E = \frac{\hbar^2(k_x^2 + k_y^2)}{2m_1^*} + \frac{\hbar^2 k_z^2}{2m_h^*}, \quad (\text{A.1})$$

where k_i is the Bloch wave number along the i axis. Due to the order-of-magnitude difference between m_1^* and m_h^* in SrTiO₃, transport is dominated by the light carriers with an effective mass of m_1^* (low mobility, or low $v^2\tau$, due to heavy effective mass outweighs any benefits from a larger density of states). Therefore, in terms of transport, the second term in Eq. A.1 is not significant, and a cylindrical geometry becomes a good model Fermi-surface for transport. Conductivity contributions from the three orthogonal cylinders will be added, neglecting avoided crossings for the sake of simplicity.

Conductivity along the x -direction in a cylindrical Fermi-surface aligned with z can be calculated by using

the solution of the Boltzmann transport equation:

$$\sigma_x = q^2 \int v_x^2(E) \tau(E) g(E) \left(\frac{-\partial f}{\partial E} \right) dE. \quad (\text{A.2})$$

By taking advantage of the rotational symmetry in the $x - y$ plane of a cylinder, v_x^2 can be replaced with $v^2/2 = E/m_1^*$ (equipartition). $g(E)$ can be derived from that of a 2D k -space ($m^*/\pi\hbar^2$) by multiplying it with the number of k -points along the z -axis ($1/a$ where a is the lattice parameter in real space):

$$g^{\text{cylinder}} = \frac{m_1^*}{a\pi\hbar^2}. \quad (\text{A.3})$$

Note that g is energy-independent as a result of the 2D nature of density of states. The conductivity of a cylindrical Fermi-surface becomes:

$$\sigma_x^{\text{cylinder}} = \frac{q^2}{a\pi\hbar^2} \int_0^\infty E \tau(E) \left(\frac{-\partial f}{\partial E} \right) dE. \quad (\text{A.4})$$

Here the transport edge (band edge) has been set to $E_t = 0$. In SrTiO₃, two cylinders (aligned along z - and y -axes) contribute to conduction in the x -direction such that $\sigma_x = 2\sigma_x^{\text{cylinder}}$, which is also the bulk isotropic conductivity.

Next, we recognize that τ should be energy-independent in order to have a model consistent with $s = 1$ that was phenomenologically found in Fig. 3. (Although possible, we avoid establishing the energy independence of τ using the deformation scattering model here so that we can discuss τ on general grounds) Therefore $\tau(E)$ is replaced with τ_l , with the subscript denoting the idea that only the light carriers are being considered. The conductivity in n-type SrTiO₃ due to light carriers becomes:

$$\begin{aligned} \sigma^{\text{SrTiO}_3} &= \frac{2e^2\tau_l}{a\pi\hbar^2} \int_0^\infty E \left(\frac{-\partial f}{\partial E} \right) dE \\ &= \frac{2e^2k_B T \tau_l}{a\pi\hbar^2} F_0(\eta), \end{aligned} \quad (\text{A.5})$$

where the $s = 1$ relation is seen. For a full derivation, one could integrate in k -space to obtain the identical result. The underlying transport function is found from this Eq. A.5, as given in Eq. 16.

From Eq. 16, it is found that the temperature dependency of conductivity is determined by $\sigma(T) \propto T\tau_l(T)F_0(\eta)$. In the degenerate limit, $F_0(\eta) \rightarrow \eta$ and $\sigma(T)$ is determined by $\tau(T)$. In the non-degenerate limit, $F_0(\eta) \rightarrow \exp(\eta)$. When $\tau \propto T^{-2}$, $\sigma \propto T^{-2}$ in the degenerate limit for a given E_F and $\sigma(T) \propto \frac{1}{T} \exp(\frac{E_F}{k_B T})$ in the non-degenerate limit.

* stephen.d.kang@gmail.com

† jeff.snyder@northwestern.edu

- ¹ N. F. Mott and E. A. Davis, *Electronic Processes in Non-Crystalline Materials*, 2nd ed. (Oxford University Press, 1979).
- ² J. T. Devreese and A. S. Alexandrov, *Reports on Progress in Physics* **72**, 066501 (2009).
- ³ J. M. Ziman, *Electrons and Phonons* (Oxford Univ. Press, 1960).
- ⁴ A. Bosman and H. van Daal, *Advances in Physics* **19**, 1 (1970).
- ⁵ Y. Long, Y. Kaneko, S. Ishiwata, Y. Taguchi, and Y. Tokura, *Journal of Physics: Condensed Matter* **23**, 245601 (2011).
- ⁶ M. H. R. Lankhorst, H. J. M. Bouwmeester, and H. Verweij, *Physical Review Letters* **77**, 2989 (1996).
- ⁷ R. E. Usiskin, T. C. Davenport, R. Y. Wang, W. Guan, and S. M. Haile, *Chemistry of Materials* **28**, 2599 (2016).
- ⁸ H. Killias, *Physics Letters* **20**, 5 (1966).
- ⁹ J. J. Kuo, S. D. Kang, K. Imasato, H. Tamaki, S. Ohno, T. Kanno, and G. J. Snyder, *Energy & Environmental Science* **11**, 429 (2018).
- ¹⁰ G. E. Pike and C. H. Seager, *Journal of Applied Physics* **50**, 3414 (1979).
- ¹¹ H. G. Reik, *Zeitschrift für Physik* **203**, 346 (1967).
- ¹² J. T. Devreese, S. N. Klimin, J. L. M. van Mechelen, and D. van der Marel, *Physical Review B* **81**, 125119 (2010).
- ¹³ D. M. Eagles and P. Lalouis, *Journal of Physics C: Solid State Physics* **17**, 655 (1984).
- ¹⁴ T. Holstein, *Annals of Physics* **8**, 343 (1959).
- ¹⁵ H. Abdalla, G. Zuo, and M. Kemerink, *Physical Review B* **96**, 241202 (2017).
- ¹⁶ E. M. Conwell, *Physical Review* **103**, 51 (1956).
- ¹⁷ R. Schmechel and H. von Seggern, *physica status solidi (a)* **201**, 1215 (2004).
- ¹⁸ P. M. Chaikin and G. Beni, *Physical Review B* **13**, 647 (1976).
- ¹⁹ W. Koshibae, K. Tsutsui, and S. Maekawa, *Physical Review B* **62**, 6869 (2000).
- ²⁰ S. D. Kang and G. J. Snyder, *Nature Materials* **16**, 252 (2017).
- ²¹ J. Bardeen and W. Shockley, *Physical Review* **80**, 72 (1950).
- ²² B. M. Askerov, *Electron Transport Phenomena in Semiconductors* (World Scientific Pub. Co. Inc., 1994).
- ²³ S. Zollner, S. Gopalan, and M. Cardona, *Journal of Applied Physics* **68**, 1682 (1990).
- ²⁴ E. Conwell and V. F. Weisskopf, *Physical Review* **77**, 388 (1950).
- ²⁵ J. W. Harrison and J. R. Hauser, *Physical Review B* **13**, 5347 (1976).
- ²⁶ H.-S. Kim, N. A. Heinz, Z. M. Gibbs, Y. Tang, S. D. Kang, and G. J. Snyder, *Materials Today* **20**, 452 (2017).
- ²⁷ S. D. Kang and G. J. Snyder, arXiv:1710.06896 [cond-mat.mtrl-sci].
- ²⁸ H. Tuller and A. Nowick, *Journal of Physics and Chemistry of Solids* **38**, 859 (1977).
- ²⁹ T. Montini, M. Melchionna, M. Monai, and P. Fornasiero, *Chemical Reviews* **116**, 5987 (2016).
- ³⁰ W. C. Chueh and S. M. Haile, *Philosophical Transactions of the Royal Society A: Mathematical, Physical and Engineering Sciences* **368**, 3269 (2010).
- ³¹ W. C. Chueh, Y. Hao, W. Jung, and S. M. Haile, *Nature Materials* **11**, 155 (2011).
- ³² J. Nell, B. J. Wood, S. E. Dorris, and T. O. Mason, *Journal of Solid State Chemistry* **82**, 247 (1989).
- ³³ T. Okuda, K. Nakanishi, S. Miyasaka, and Y. Tokura, *Physical Review B* **63** (2001).
- ³⁴ S. Ohta, T. Nomura, H. Ohta, and K. Koumoto, *Journal of Applied Physics* **97**, 034106 (2005).
- ³⁵ J. Mannhart and D. G. Schlom, *Science* **327**, 1607 (2010).
- ³⁶ A. F. Santander-Syro, O. Copie, T. Kondo, F. Fortuna, S. Pailhès, R. Weht, X. G. Qiu, F. Bertran, A. Nicolaou, A. Taleb-Ibrahimi, P. L. Fèvre, G. Herranz, M. Bibes, N. Reyren, Y. Apertet, P. Lecoeur, A. Barthélémy, and M. J. Rozenberg, *Nature* **469**, 189 (2011).
- ³⁷ R. Waser and M. Aono, *Nature Materials* **6**, 833 (2007).
- ³⁸ M. Ahrens, R. Merkle, B. Rahmati, and J. Maier, *Physica B: Condensed Matter* **393**, 239 (2007).
- ³⁹ A. Rothschild, W. Meneskluou, H. L. Tuller, and E. Ivers-Tiffée, *Chemistry of Materials* **18**, 3651 (2006).
- ⁴⁰ H. Muta, K. Kurosaki, and S. Yamanaka, *Journal of Alloys and Compounds* **350**, 292 (2003).
- ⁴¹ R. Moos, A. Gnudi, and K. H. Härdtl, *Journal of Applied Physics* **78**, 5042 (1995).
- ⁴² H. P. R. Frederikse, W. R. Thurber, and W. R. Hosler, *Physical Review* **134**, A442 (1964).
- ⁴³ T. Hara and K. Shinozaki, *Japanese Journal of Applied Physics* **50**, 065807 (2011).
- ⁴⁴ P. Roy, V. Pal, and T. Maiti, *Ceramics International* **43**, 12809 (2017).
- ⁴⁵ C. Ang, J. R. Jurado, Z. Yu, M. T. Colomer, J. R. Frade, and J. L. Baptista, *Physical Review B* **57**, 11858 (1998).
- ⁴⁶ G. Campet, S. Z. Wen, C. Puprichitkun, J. P. Manaud, and J. Claverie, *Physica Status Solidi (a)* **103**, 175 (1987).
- ⁴⁷ E. Mikheev, S. Raghavan, J. Y. Zhang, P. B. Marshall, A. P. Kajdos, L. Balents, and S. Stemmer, *Scientific Reports* **6**, 20865 (2016).
- ⁴⁸ F. W. Lytle, *Journal of Applied Physics* **35**, 2212 (1964).
- ⁴⁹ C. A. Kukkonen, *Physical Review B* **18**, 1849 (1978).
- ⁵⁰ V. F. Gantmakher, *Reports on Progress in Physics* **37**, 317 (1974).
- ⁵¹ L. Feng, T. Shiga, and J. Shiomi, *Applied Physics Express* **8**, 071501 (2015).
- ⁵² J.-S. Zhou, J. B. Goodenough, and B. Dabrowski, *Physical Review Letters* **94** (2005).
- ⁵³ A. Sakai, T. Kanno, S. Yotsuhashi, H. Adachi, and Y. Tokura, *Japanese Journal of Applied Physics* **48**, 097002 (2009).
- ⁵⁴ D. Oka, Y. Hirose, S. Nakao, T. Fukumura, and T. Hasegawa, *Physical Review B* **92** (2015).
- ⁵⁵ I. Nagai, N. Shirakawa, S. ichi Ikeda, R. Iwasaki, H. Nishimura, and M. Kosaka, *Applied Physics Letters* **87**, 024105 (2005).
- ⁵⁶ X. Lin, B. Fauque, and K. Behnia, *Science* **349**, 945 (2015).
- ⁵⁷ D. Keroack, Y. Lepine, and J. L. Brebner, *Journal of Physics C: Solid State Physics* **17**, 833 (1984).
- ⁵⁸ S. Saraf, I. Riess, and A. Rothschild, *Advanced Electronic Materials* **2**, 1500368 (2016).
- ⁵⁹ G. H. Jonker, *Philips Research Reports* **23**, 131 (1968).
- ⁶⁰ A. F. Mayadas and M. Shatzkes, *Physical Review B* **1**, 1382 (1970).
- ⁶¹ W. Steinhögl, G. Schindler, G. Steinlesberger, and M. Engelhardt, *Physical Review B* **66**, 075414 (2002).
- ⁶² T. Kanno, H. Tamaki, H. K. Sato, S. D. Kang, S. Ohno, K. Imasato, J. J. Kuo, G. J. Snyder, and Y. Miyazaki, *Applied Physics Letters* **112**, 033903 (2018).
- ⁶³ A. J. Bosman and C. Crevecoeur, *Physical Review* **144**, 763 (1966).

- ⁶⁴ H. Wang, C. Wang, W. Su, J. Liu, H. Peng, J. Zhang, M. Zhao, J. Li, N. Yin, and L. Mei, *Journal of Alloys and Compounds* **486**, 693 (2009).
- ⁶⁵ A. V. Kovalevsky, A. A. Yaremchenko, S. Populoh, P. Thiel, D. P. Fagg, A. Weidenkaff, and J. R. Frade, *Physical Chemistry Chemical Physics* **16**, 26946 (2014).
- ⁶⁶ K. Imasato, S. D. Kang, S. Ohno, and G. J. Snyder, *Materials Horizons* **5**, 59 (2018).
- ⁶⁷ S. D. Kang, J.-H. Pöhls, U. Aydemir, P. Qiu, C. C. Stoumpos, R. Hanus, M. A. White, X. Shi, L. Chen, M. G. Kanatzidis, and G. J. Snyder, *Materials Today Physics* **1**, 7 (2017).
- ⁶⁸ M. Statz, D. Venkateshvaran, X. Jiao, S. Schott, C. R. McNeill, D. Emin, H. Siringhaus, and R. D. Pietro, *Communications Physics* **1** (2018).